REVISTA INTERDISCIPLINAR DE PESQUISA EM ENGENHARIA

CILAMCE 2016
XXXVII IBERIAN LATIN AMERICAN CONGRESS ON COMPUTATIONAL METHODS IN ENGINEERING
BRASÍLIA - DF - BRAZIL

BOUNDARY TREATMENT TECHNIQUES IN SMOOTHED PARTICLE HYDRODYNAMICS: IMPLEMENTATIONS IN FLUID AND THERMAL SCIENCES AND RESULTS ANALYSIS

Carlos Alberto Dutra Fraga Filho[1]

Julio Tomás Aquije Chacaltana[2]

cadff1@gmail.com

julio.chacaltana@ufes.br

[1] Federal Institute of Education, Science and Technology of Espírito Santo – Mechanical Engineering Coordination – Av. Vitória, 1729 – 29040-620 – Jucutuquara – Vitória – ES – Brazil

[2] Federal University of Espírito Santo – Environmental Engineering Department – Laboratory of Simulation of Free Surface Flows (LABESUL) — Av. Fernando Ferrari, 514 – 29075-910 – Goiabeiras – Vitória – ES – Brazil

Abstract. *Appropriate boundary treatment technique is one of the greatest challenges found in the Smoothed Particle Hydrodynamics (SPH) Lagrangian method. This paper focuses on the treatment of different boundary condition techniques and their implementation in the SPH code developed by the authors. The boundary conditions implemented and tested in this work involve the use of virtual particles, repulsive force, geometric reflection, and dynamic particle treatments. A code was written in Fortran language in order to solve the system of algebraic equations that result from the application of the SPH method in the discretization of the conservation equations. The implemented boundary conditions are tested and the numerical results are compared with results from non-commercial codes and analytical ones. In general, the numerical results obtained in the present work are in agreement with those reported in the literature.*

Keywords: *Boundary conditions, SPH, Heat transfer, Thermal sciences, Fluid mechanics.*

1 INTRODUCTION

Traditionally, Partial Differential Equations (PDEs) are written in a Eulerian reference frame and it is often necessary to use meshes/grids (structured or unstructured) such as finite volumes, finite differences, and finite elements to solve them. Recently, a meshless Lagrangian method called Smoothed Particle Hydrodynamics (SPH) has been used to solve the fluid movement and the transport of physical properties from one region to another one by following a definite number of fluid particles.

This Lagrangian particle method was originally developed by Lucy (1977) and Gingold and Monaghan (1977) for modelling astrophysical phenomena. By employing particles, the SPH method easily discretizes complex geometries, refines the domain, and captures the free surfaces and their topological changes. An appropriate treatment of the boundary conditions is reported as one of the difficulties in using this method. SPH has been employed in computational fluid dynamics and mass/heat transfer for the numerical solution of a system of differential equations given by the physical laws of conservation of mass and energy and momentum balance. It has been shown to be an alternative to the mesh methods (which discretize the domain through a fixed mesh/grid in space, causing difficulty in capturing the free surfaces and their topological changes requiring the extra effort of remeshing in every numerical iteration). In this context, SPH presents advantages such as the fact that there is no need for either grid remeshing at each numerical iteration or time step (decreasing the computational cost) or identification of the free surface by particles, which evolve as time progresses.

In this context, SPH presents advantages such as the fact that there is no need for either grid remeshing at each numerical iteration or time step (decreasing the computational cost) or identification of the free surface by particles, which evolve as time progresses.

In this work, the virtual particle, repulsive force, geometric reflection, and dynamic particle techniques for the treatment of boundary conditions were tested. In doing so, a set of physical problems involving the heat diffusion in a flat plate, still fluid within an immobile reservoir, a shear-driven cavity, the propagation of water waves over a flat beach, and dam break are studied. A code written in FORTRAN language was developed and implemented in the research. The non-commercial codes FUNWAVE and SPHysics have assisted in the simulations. The numerical results obtained by SPH showed a good agreement with the analytical, experimental, and numerical results reported in the literature.

Other methods for the treatment of boundaries are also used in SPH. Among them we can mention the semi-analytical (Kulasegaram et al., 2004; Ferrand et al., 2012) and semi-unified analytical boundary conditions (Leroy et al. 2012) and a modified method with virtual particles based on a local symmetry approach (Fourtakas et al. 2015).

This paper is organized in sections as follows. In Section 2, a brief description of the SPH method is given. Details of the treatment of the boundary conditions are described in Section 3. The set of problems, their results, and a discussion of their results are presented and discussed in Section 4. Finally, the conclusions are given in Section 5.

2 FUNDAMENTALS OF SMOOTHED PARTICLE HYDRODYNAMICS METHOD

For the solution of conservation differential equations, the SPH method discretizes the domain into a finite number of particles. The values of the physical properties of the reference particles are obtained by interpolation of the properties of neighbouring particles with the use of smoothing functions (kernels). The particles are delimited by a domain of influence (at a maximum distance $\mathrm{k}h$ from the fixed particle considered) that defines an area of influence in which there is a contribution of the neighbouring particles to the approximations of the physical properties of the reference particle, as shown in Fig. 1.

In the SPH method, different kernels can be used, and to be considered suitable for interpolation, each must have certain properties: smoothness, positivity, symmetry, convergence, decay, compact support, and normalization within the domain of influence (Liu and Liu, 2003). Common kernels used in the interpolations are presented in Fraga Filho and Chacaltana (2014).

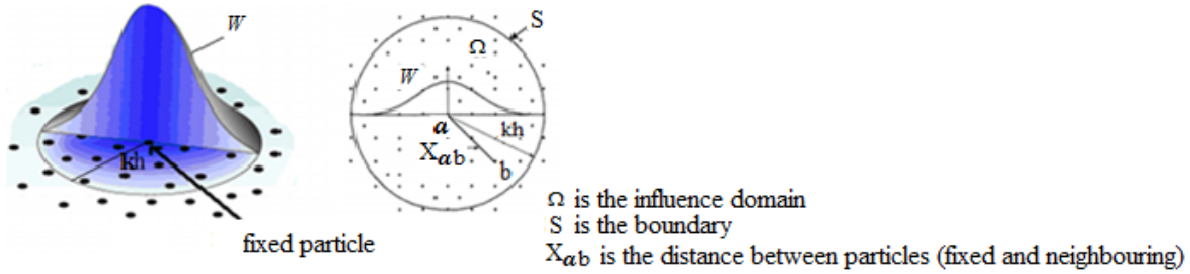

Figure 1. Graphical representation of the domain of influence. The fixed particle (reference) has neighbouring particles (b) within the domain of influence. The kernel (W) ensures a greater contribution of the nearest neighbouring particles to the value of the physical property of the reference particle.

SPH approaches physical properties (such as density), gradients (as pressure gradients), divergence (such as velocity divergence), and Laplacians (such as temperature and velocity Laplacians) related to fluid flow, with a second order error.

The general expressions for approximations of a scalar physical property, A_a, its gradient (symmetric form) and its Laplacian (Fraga Filho and Chacaltana, 2014) are given by Eqs. (01), (02), and (03) below:

$$A_a = \sum_{b=1}^{n} m_b \frac{A_b}{\rho_b} W\left(\boldsymbol{X}_a - \boldsymbol{X}_b, h\right) \tag{01}$$

$$\nabla A_a = -\rho_a \sum_{b=1}^{n} m_b \left(\frac{A_a}{\rho_a^2} + \frac{A_b}{\rho_b^2}\right) \nabla W\left(\boldsymbol{X}_a - \boldsymbol{X}_b, h\right) \tag{02}$$

$$\nabla^2 A_a = 2\sum_b \frac{m_b}{\rho_b}\left(A_a - A_b\right) \frac{\boldsymbol{X}_a - \boldsymbol{X}_b}{\left|\boldsymbol{X}_a - \boldsymbol{X}_b\right|^2} . \nabla W\left(\boldsymbol{X}_a - \boldsymbol{X}_b, h\right) \tag{03}$$

The divergence of a physical vectorial property, $\boldsymbol{A}_a$, can be calculated by Eq. (04).

$$\nabla.\boldsymbol{A}_a = \frac{1}{\rho_a}\sum_{b=1}^{n} m_b \left(\boldsymbol{A}_b - \boldsymbol{A}_a\right).\nabla W\left(\boldsymbol{X}_a - \boldsymbol{X}_b, h\right) \tag{04}$$

In the expressions above, ∇ is the mathematical vector operator nabla; A_a is the scalar physical property approximated (it refers to fixed particle a); A_b is the scalar physical property of the neighbouring particle b; $\boldsymbol{A}_a$ is the vector physical property of the reference particle; $\boldsymbol{A}_b$ is the vector physical property of the neighbouring particle b; n is the number of neighbouring particles within the influence domain; m_b is the mass of particle b; W is the kernel; h is the support radius; $\boldsymbol{X}_a$ and $\boldsymbol{X}_b$ are the positions of the fixed and neighbouring particles, respectively; and ρ_b is the density of the neighbouring particle b.

The time evolution of the physical properties carried by matter is given by Eqs. (05) to (07) for the specific mass, velocity, and internal energy, respectively. Table 1 shows these equations written in the Lagrangian frame of reference and their approximations in the SPH method in a viscous and compressible fluid.

Table 1 – Differential Equations and SPH Approximations

Differential Equation (Continuum)	SPH Approximation (Domain discretized by particles)
Mass conservation: $\dfrac{\mathrm{d}\rho}{\mathrm{dt}} = -\rho\nabla.\mathbf{v}$	$\dfrac{\mathrm{d}\rho_a}{\mathrm{dt}} = \sum_{b=1}^{n} m_b \mathbf{v}_{ab}.\nabla W\left(\boldsymbol{X}_a - \boldsymbol{X}_b, h\right)$ (05)
Momentum balance: $\dfrac{\mathrm{d}\mathbf{v}}{\mathrm{dt}} = -\dfrac{\nabla P}{\rho} + \upsilon\nabla^2\mathbf{v} + \mathbf{g}$	$\dfrac{\mathrm{d}\mathbf{v}_a}{\mathrm{dt}} = \sum_{b=1}^{n} m_b \left(\dfrac{P_a}{\rho_a^2} + \dfrac{P_b}{\rho_b^2}\right)\nabla W\left(\boldsymbol{X}_a - \boldsymbol{X}_b, h\right) +$ $+2\upsilon_a \sum_{b=1}^{n} \dfrac{m_b}{\rho_b}\mathbf{v}_{ab}\dfrac{\left(\boldsymbol{X}_a - \boldsymbol{X}_b\right)}{\left\lvert\boldsymbol{X}_a - \boldsymbol{X}_b\right\rvert^2}.\nabla W\left(\boldsymbol{X}_a - \boldsymbol{X}_b, h\right) + \mathbf{g}$ (06)
Energy conservation: $\dfrac{\mathrm{de}}{\mathrm{dt}} = \dfrac{1}{\rho}\left(-P.\nabla\mathbf{v} + \varepsilon_{\mathrm{v}} + \nabla.\,\mathbf{q} + q_H\right)$	$\dfrac{\mathrm{de}_a}{\mathrm{dt}} = \dfrac{1}{\rho}\left[-P_a\sum_{b=1}^{n} m_b \mathbf{v}_{ab}.\,\nabla W\left(\boldsymbol{X}_a - \boldsymbol{X}_b, h\right) + \varepsilon_{\mathrm{v}} + \right.$ $\left. +\nabla.\,\mathbf{q} + q_H\right]$ (07)

where $\mathbf{v}$ is the velocity; $\mathbf{g}$ is the gravity; υ is the kinematic fluid viscosity; P is the pressure; t is the time; e is the specific internal energy; ε_{v} is the energy dissipation per volume unit; $\mathbf{q}$ is the conduction heat flux; q_H is the heat generated by other sources per volume unit; $\boldsymbol{X}_{ab} = \boldsymbol{X}_a - \boldsymbol{X}_b$; $\mathbf{v}_{ab} = \mathbf{v}_a - \mathbf{v}_b$; and a and b are subscripts that refer to fixed and neighbouring particles, respectively.

In the SPH method, created for the simulation of compressible fluid, the pressure is an explicit function of the local density of the fluid. In the dynamic case, the compressible fluid approximates an incompressible fluid through a quasi-compressible fluid and pressure is calculated by an equation of state. In the researches, the Tait equation was used to predict the dynamic pressure (Batchelor, 2000):

$$P_{dyn(a)} = B\left(\left(\frac{\rho_a}{\rho_o}\right)^{\gamma} - 1\right) \tag{08}$$

where $P_{dyn(a)}$ is the dynamic pressure on the fixed particle; ρ_a is the density of the fixed particle; ρ_o is the density of the fluid at rest; $\gamma = 7$; and B is the term related to the density fluctuations of the fluid.

The prediction of physical properties of particles for the subsequent instant of numerical simulation is performed by a temporal integration method. The Courant-Friedrichs-Lewy (CFL) stability criterion was applied in the time step setting to ensure convergence of results (Courant et al., 1967).

3 BOUNDARY CONDITIONS

In this section, the techniques for the treatment of boundary conditions will be presented. In the final subsection, the inconsistency of the SPH in regions near the boundaries will be discussed.

3.1 Virtual particles and repulsive boundary conditions

One way to effect the boundary treatment of solid closed contours in SPH consists in the use of virtual particles on the contours or near them (in an extended region of the domain). Repulsive forces arising from the interaction between virtual and fluid particles prevent the latter from exceeding the contours and escaping the domain.

According to their positions, the virtual particles are classified into two categories: type I, located on the contour, and type II, located outside the contour. Figure 2 shows both types of virtual particles in the simulation of solid walls.

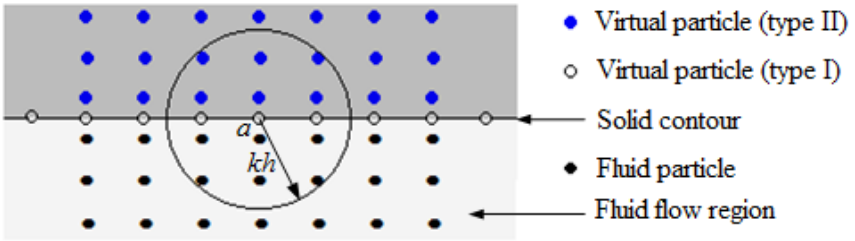

Figure 2. Schematic illustration of the solid contour region. Arrangement of the virtual particles of type I (a line on the contour) and the virtual particles of type II (in an extended area beyond the domain).

The repulsive force exerted by the virtual particle on the fluid particle is calculated by analogy with the Lennard-Jones molecular force (Rapaport, 2004). A virtual particle of type I that is in the vicinity of a fluid particle, near the boundary, exerts a force in the direction of the line connecting both particles' centres ($\boldsymbol{F}_{ij}$):

$$\boldsymbol{F}_{ij} = \begin{cases} D\left[\left(\dfrac{r_0}{|\boldsymbol{r}_{ij}|}\right)^{n_1} - \left(\dfrac{r_0}{|\boldsymbol{r}_{ij}|}\right)^{n_2}\right]\dfrac{\boldsymbol{X}_{ij}}{|\boldsymbol{r}_{ij}|^2}, & if \quad \dfrac{r_0}{|\boldsymbol{r}_{ij}|} \le 1 \\ 0, \quad if \quad \dfrac{r_0}{|\boldsymbol{r}_{ij}|} > 1. \end{cases} \tag{09}$$

where $|\boldsymbol{r}_{ij}|$ is the distance between a virtual particle and a fluid particle; n_1 and n_2 are parameters that are usually equal to 12 and 4, respectively; D is a parameter that depends on each problem and must be of the same order of magnitude as the square of the highest flow velocity; r_0 is the cutoff distance; and $\boldsymbol{X}_{ij}$ is the difference between the position vectors of the virtual particle and the fluid particle.

The sum of the contributions to the force of each virtual particle on the fluid particle will be the resultant force that will keep the latter within the domain.

After the initial setup of all particles in the domain, physical properties can be imposed on the virtual particles. From the initial properties of these particles, approximate properties can be obtained for the fluid particles. It is not always necessary to implement the Lennard-Jones repulsive force; this definition depends on the analysis of each problem studied.

In this work, there are cases where boundaries received treatments with the use of virtual particles of types I and II with or without the implementation of that repulsive force.

3.2 Geometric Boundary Conditions

In the geometrical boundary conditions, collisions of the particles of fluid against the solid walls (considered as well-defined planes) are implemented. Figure 3 shows the initial and final positions, C_0 and C_f, of the centre of mass of a particle after it has collided successively with two planes (A and B) in a numerical iteration. The point C_1 is the final position that would be achieved by the particle mass centre if there were no walls delimiting the field.

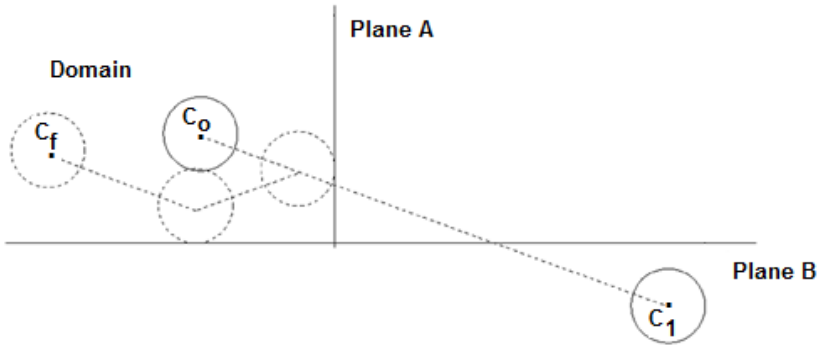

Figure 3. Collisions experienced by a particle in a time step.

SPH is a model of one particle; that is, collisions between particles are not considered. An algorithm for the study of collisions and trajectories of the particles that collide against the solid walls of the domain has been implemented. After carrying out the temporal integration and obtaining the position of the centre of mass of each fluid particle by the SPH method (in

the situation in which there are no walls delimiting the domain), the collision algorithm, based on mathematical and geometry fundamentals, brings the particles back into the domain. This is based on the fact that the fluid particles could not escape the domain due to the presence of the predefined geometrical planes. The degree of elasticity of the collisions was measured by a coefficient of restitution of kinetic energy (CR).

When the collision of a particle against a plane was detected, and the particle velocity was obtained by the SPH method, this particle velocity was corrected immediately after the impact, as follows:

$$(v_{col})_i = CR \times (v_p)_i \tag{10}$$

where $(v_p)_i$ and $(v_{col})_i$ are the magnitudes of the components of the particle velocities in the direction i before and after the collision, respectively; $i \in (x, y)$.

After the collision, the sense of the particle velocity component perpendicular to the wall is altered. The sense of the velocity component parallel to the wall remains unaltered.

3.3 Dynamic Boundary Conditions

Under the dynamic boundary conditions, particles located at the boundaries obey the mass conservation, momentum balance, energy conservation, and Tait equations (the last is used for the prediction of dynamic pressures in the fluid particles). The fixed particles in the contours can be fixed or can have movement (being governed by an external function imposed in the case of the existence of wave-makers and gates, among others (Gomez-Gesteira et al., 2010; Gomez-Gesteira et al., 2012). When a fluid particle approaches the solid outlines, there is an increase in density and pressure related to a boundary particle. These increases cause a growth in the magnitude of the repulsion force exerted on the fluid, due to the increase in the value of the term P/ρ^2 in the momentum balance equation, and as a result the fluid particles are kept within the domain. Figure 4 shows the interaction between particles fixed on the contour and a fluid particle that approaches the border, as well the effects of the approximation on the pressure and density of the boundary particles.

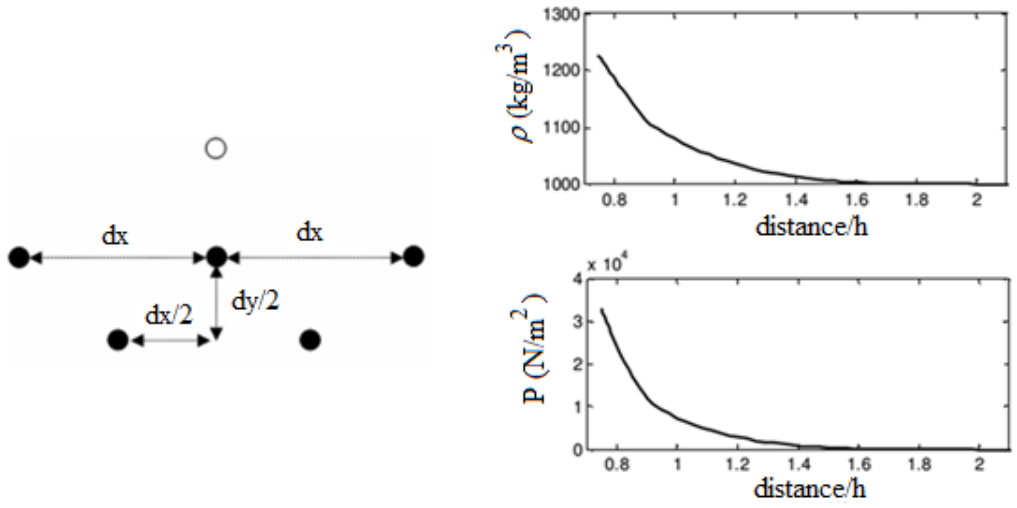

(a) (b)

Figure 4. (a) Interaction between particles fixed on the contour (circles in black arranged in a staggered manner) and a fluid particle that approaches the border (hollow circle). (b) Increases in the density and pressure of a boundary particle, with the approximation of a fluid particle.

When there are open boundaries, periodicity is implemented to keep the particles within the domain throughout the simulation time.

3.4 Particle Inconsistency

Particles near the boundaries do not have complete domains of influence, which causes truncation of the kernel and consequent lower accuracy in the interpolations (Liu and Liu, 2010). This phenomenon is known as particle inconsistency. Figure 5 shows the occurrence of the truncation of the kernel in the coordinate polar system.

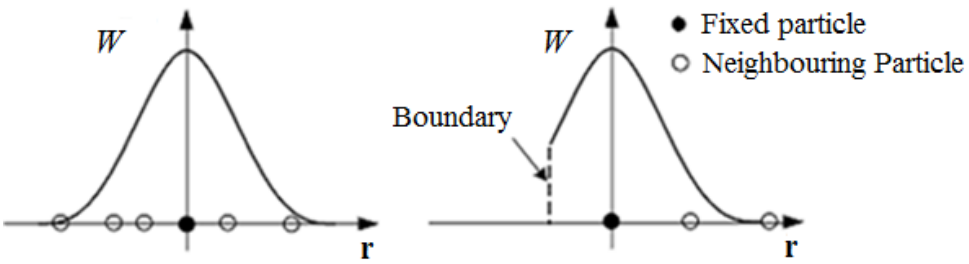

(a) (b)

Figure 5. Domain of influence in a polar coordinate system. (a) Complete and (b) incomplete. It is possible see that the kernel is not defined in a whole domain.

In the border regions, as shown in Fig. 5 (b), the kernel consistency is not guaranteed. There is not a full domain of influence and the kernel is truncated. A correction method based on the Taylor series called the Corrected Smoothed Particle Method (CSPM) is used in the correction of the inconsistency (Chen et al., 1999).

4 PHYSICAL PROBLEMS

4.1 Heat Diffusion in a Homogeneous Flat Plate

The equation that governs the energy transfer in the absence of pressure fields and energy dissipation is presented below:

$$\rho \frac{de}{dt} = \nabla . \boldsymbol{q} + q_H \tag{11}$$

$$\boldsymbol{q} = k \nabla T \tag{12}$$

where e is the specific energy, ρ is the density, t is the time, $\boldsymbol{q}$ is the heat flux, and q_H is the heat source.

In the absence of heat sources and a thermal conductivity constant, under steady state, Eq. (13), written according to the Lagrangian referential, becomes:

$$\frac{\partial^2 T}{\partial x^2}+\frac{\partial^2 T}{\partial y^2}=0 \tag{13}$$

The dimensions and boundaries of the plate are shown in Fig. 7. The whole domain has temperature T_0 equal to $0°C$, at the initial time; that is, the initial temperature is uniform. The prescribed boundary conditions (Dirichlet boundary conditions) are imposed. The initial and boundary conditions are presented below.

The initial condition is:

$$T(\mathrm{x},\mathrm{y})=T_0 \quad (0<\mathrm{x}<1 \text{ and } 0<\mathrm{y}<1), \tag{14}$$

The boundary conditions are:

$$T(0,\mathrm{y})=0°C \quad (0\le \mathrm{y}\le 1), \tag{15}$$

$$T(1,\mathrm{y})=0°C \quad (0\le \mathrm{y}\le 1), \tag{16}$$

$$T(\mathrm{x},0)=T_S=100°C \quad (0<\mathrm{x}<1), \tag{17}$$

$$T(\mathrm{x},1)=0°C \quad (0<\mathrm{x}<1). \tag{18}$$

Pletcher et al. (2013) employed the technique of the separation of variables to obtain the solution by series for Eq. (13):

$$T(\mathrm{x},\mathrm{y})=\sum_{N=1}^{\infty} A_N \sin(N\pi \mathrm{x})\sinh[N\pi(\mathrm{y}-1)] \tag{19}$$

$$\text{where} \quad A_N=\frac{2T_S}{N}\frac{[(-1)^N-1]}{\sinh(k)}\ , \tag{20}$$

$T_S=T(\mathrm{x},0)$ is the temperature at the lower boundary, and N is the number of points employed in the series.

The solution obtained for the series was used as a standard for comparison with the results obtained by SPH.

In the numerical code based on SPH, the particle mass centres were placed in the domain separated by a distance $d\mathrm{x}=d\mathrm{y}=1/n_p$ (n_p is the number of particles on each side of the plate). The particles' positions did not change with time. Five different values of n_p (50, 60, 70, 80, and 90) were employed.

In the defining of the boundaries, virtual particles of type I were fixed at the contours at a ratio of two virtual particles for each real particle and the temperatures of the sides of the plate were attributed to them. Virtual particles' properties were not subject to interpolations to predict their temperatures (Dirichlet boundary conditions). The particles inside the domain had their temperatures initialized to 0 °C and the thermal diffusivity was defined as 1.0 m^2/s, which was held constant for all simulations. The influence domain ($\mathrm{k}h$) was defined as $2.5\,d\mathrm{x}$, which was invariable during simulations. The time step was 1.0 x 10^{-5} s.

The calculation of the Laplacian of temperature for each iteration was done explicitly, in a polar coordinate system, by solving the following equation:

$$\left(\frac{\partial^2 T_a}{\partial \mathrm{x}^2}+\frac{\partial^2 T_a}{\partial \mathrm{y}^2}\right)^m = 2\sum_{b=1}^{n}\frac{m_b}{\rho_b}\left[T(X_a)^m - T\left(X_b\right)^m\right].\frac{\partial W(r,h)}{\partial r}\frac{1}{r_{ab}} \tag{21}$$

where

m is the current time step, b is the subscript indicating each neighbouring particle of the fixed particle, which is denoted by the subscript a, n is the number of particles within the domain of influence, $r_{ab} = \left|\boldsymbol{X}_a - \boldsymbol{X}_b\right|$ is the distance between two particles, and r is the radial direction.

Simulations were carried out starting from the transient until the steady state was reached. Different combinations of numbers of particles (50, 60, 70, 80, and 90 per side of the flat plate) and kernels were used (Fraga Filho and Chacaltana, 2014). Figure 6 shows the initial distribution of 50 × 50 particles in the domain (and the prescribed temperatures at the boundaries, attributed to the virtual particles) and the temperature distribution when the steady state was reached (t = 0.431 s).

For internal regions of the domain, the approximation of the Laplacian of the temperature by the SPH method gave results that were in agreement with the analytical solution.

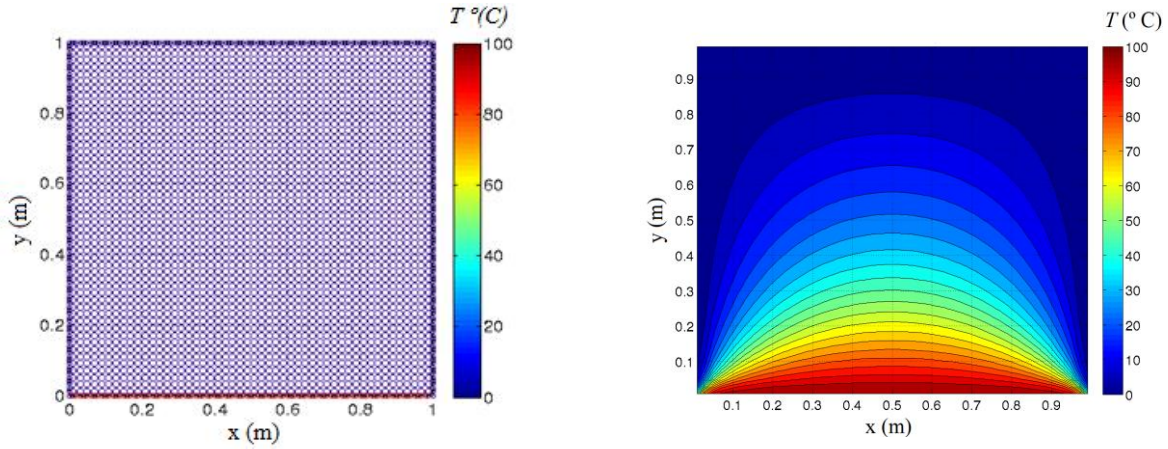

(a) (b)

Figure 6. (a) Initial distribution of 50 × 50 particles in the domain and the prescribed temperatures at the boundaries (attributed to the virtual particles). (b) Temperature distribution when the steady state was reached (a cubic spline kernel was employed).

In all combinations of particle numbers and kernels, particle inconsistency was seen in the regions near the boundaries. The largest relative errors found in the steady state (obtained from the analysis of the differences between the analytical solution and the SPH numerical results) occurred in a few positions of the lower corners of the flat plate. Figure 7 shows these larger relative errors for different combinations of particle numbers and kernels.

Smaller differences in temperatures in regions close to the boundaries were observed when a kernel of higher degree was utilized (quintic spline), except for the distribution with 3600 particles (Fraga Filho and Chacaltana, 2014).

From the analysis of the results, we can conclude that to achieve better results it is necessary to perform a correction of the temperature values in regions near the contours.

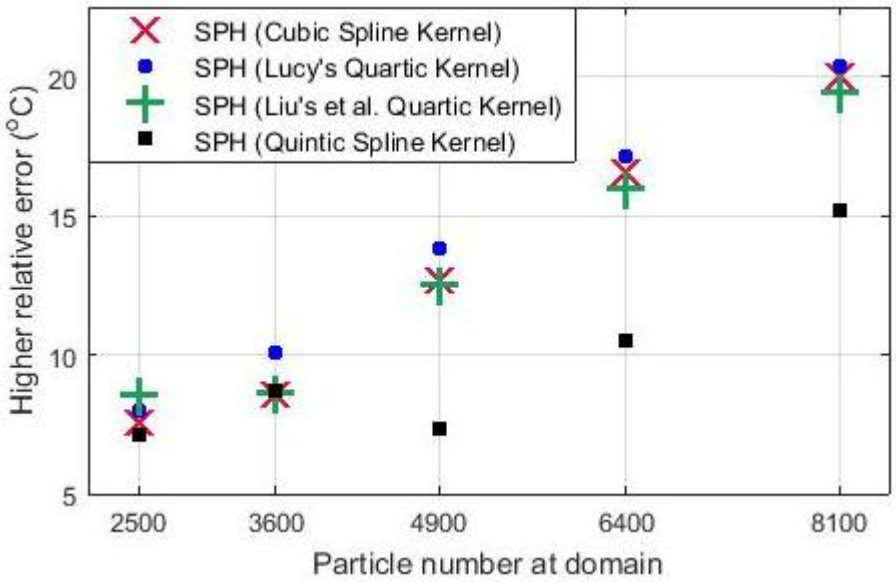

Figure 7. Behaviour of the higher relative error.

4.2 Still liquid within an immobile reservoir

The solution for a Newtonian, incompressible, and isothermal fluid at rest within an immobile reservoir is well known. Application of the macroscopic view and continuum theory (where the molecular motion of the fluid is not considered) allowed the Navier-Stokes equations – mass conservation and momentum balance – to be obtained in the mathematical modelling of the problem. Following this theory, the movement of particles cannot occur at any instant of time. The origin of the frame of reference, that has a positive vertical orientation pointing upwards, is located at the bottom of the reservoir. The analysis has been performed in a 2D domain.

Application of the concept of the modified pressure (P_{mod}), as shown in Eq. (22), which is null in the hydrostatic case, allows the momentum balance equation to be written, as Eq. (23).

$$P_{\text{mod}} = (P - P_o) - \rho g(H - \text{y}) = 0 \tag{22}$$

where P_o is the reference pressure and H is the fluid level in the reservoir.

$$\frac{\text{d}\mathbf{v}_a}{\text{d}t} = \sum_{b=1}^{n} m_b \left(\frac{P_{\text{mod}(a)}}{{\rho_a}^2} + \frac{P_{\text{mod}(b)}}{{\rho_b}^2} \right) \nabla W(\boldsymbol{X}_a - \boldsymbol{X}_b, h) + \\ + 2\upsilon_a \sum_{b=1}^{n} \frac{m_b}{\rho_b} (\mathbf{v}_a - \mathbf{v}_b) \frac{\boldsymbol{X}_a - \boldsymbol{X}_b}{\left| \boldsymbol{X}_a - \boldsymbol{X}_b \right|^2} . \nabla W(\boldsymbol{X}_a - \boldsymbol{X}_b, h) \tag{23}$$

where the subscripts a and b refer to the properties of the reference and neighbouring particles, respectively.

The hydrostatic problem consists of a tank that is at rest, open to the atmosphere, and filled with a liquid, as shown in Fig. 8 (a). The initial distribution of the particles in the domain was performed on a regular basis with 50 particles per side of the tank with dimensions of 1.00 × 1.00 m, or 2500 fluid particles in total. The lateral distance between the centres of mass of two particles was $dx = dy = 0.02$ m. The radius of the influence domain (kh, for each particle) was defined as 0.05 m and was invariable during simulations. The number of particles within that was 21. The boundary treatment was done with the use of virtual particles of type II. Three rows and three columns of this type of particle were added on the domain side, making a total of 636 virtual particles. It was ensured that the kernel truncation would not occur (a complete domain of influence on all fluid particles was ensured). The fluid particles were evenly distributed and, in this manner, particle inconsistency next to the border regions was avoided. Figure 8 (b) shows the initial particle distribution in the domain and the distribution of hydrostatic pressure on the fluid particles. The cubic spline kernel has been used.

The modified pressures for all particles (fluid and virtual) at rest were initialized to zero. The cubic spline kernel was used in the simulations. The time step employed was 1.00×10^{-4} s and the Courant-Friedrichs-Lewy criterion for convergence was obeyed (Courant, Friedrichs and Lewy, 1967). The temporal integration of the positions and velocities has been done by the Eulerian method (the Runge-Kutta first-order method).

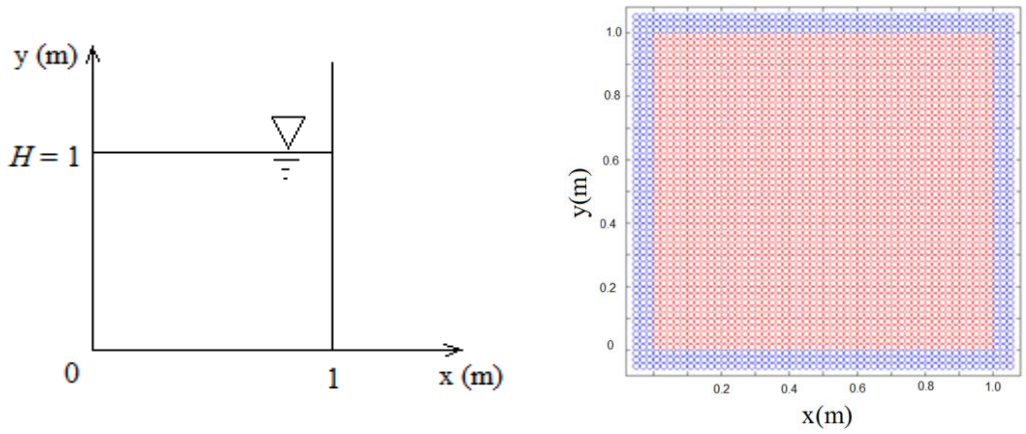

(a) (b)

Figure 8. (a) Open reservoir containing a uniform, incompressible, and isothermal liquid. (b) Initial distribution of fluid particles (red) and virtual particles (blue). The latter are in an expanded region of the domain.

After the solution of Eq. (23) and updating of the positions and velocities of the particles by the temporal integration, for each numerical iteration, those remained unchanged, and the hydrostatic equilibrium have been maintained. Thus, the modified pressure field was maintained with a null value at the beginning of each new iteration so that the particles would remain at rest.

In the approximations to a function and its derivatives taken by the SPH method there are errors (Fraga Filho, 2014; Vaughan, 2008). When the SPH was applied without the use of modified pressure to obtain the approximations for the pressure and viscosity forces, terms

which were present in the momentum balance equation and which were added to the gravitational force, it caused small mistakes to appear. Despite the small orders of magnitude of these errors, they spread and increased during the numerical simulation. By using the modified pressure, the sum of the gravitational force and the terms approximated by the SPH for surface forces has been avoided. Thus, the errors have been eliminated and there was a coincidence between the initial positions of the particles and the positions obtained by the SPH method throughout the simulation.

4.3 Shear-Driven Cavity

The cavity consists of a square box (equal height and width) within which an incompressible and Newtonian fluid is forced to move by the box cover movement (which has a constant velocity). The velocities of the remaining walls of the box are null. The no-slip condition was applied on the walls. The mass conservation and momentum balance equations, Eqs. (05) and (06), were employed to achieve the solution of the problem.

The sides of the square cavity were 1×10^{-3} m. In all simulations, 40 particles were used per side, distributed within the cavity, and 80 virtual particles of type I were used on each of the walls. The radius of the domain of influence was defined as $1.25dx$ (invariable). The velocities of particles in the cavity simulations started at zero. The velocities of the virtual particles on the box cover were initialized and maintained at a constant velocity during the simulations. The fluid flowing in the cavity was water with a density of 10^3 kg/m^3 and kinematic viscosity of 10^{-6} m^2/s. A model to assess the turbulence effects was not included (a possible error factor for higher Reynolds numbers) and gravity was not considered.

The Gaussian kernel was used in the simulations (Monaghan, 1992). Repulsive boundary conditions were employed, with the implementation of the Lennard-Jones force. The parameters n_1 and n_2 in Eq. (11) were taken as 12 and 4, respectively. The cutoff distance was 1.25×10^{-5} m and the parameter D was assigned a value of 1.0×10^{-2} m^2/s^2. The time step was 5×10^{-5} s. Kernel truncation occurred for the particles near the cavity walls. Renormalization of the particle density has been performed during the simulations. The SPH approximations for the pressure gradients near the contours were not corrected. Simulations were performed for Reynolds numbers ranging from 0.01 to 100.00; that is, different velocities of the box cover of the cavity were employed (Pinto et al., 2011; Pinto, 2013).

In all simulations, the formation of a primary vortex occurred in the upper region of the cavity when the stationary condition was reached. There was only a major circulation, without secondary circulations in the corners, due to the range of Reynolds numbers used. Figure 9 shows the initial particle distribution in the domain and on the contours, and the streamlines, velocity field, and primary vortex formed. The positions of the primary vortices were compared to the literature results for Reynolds numbers ranging from 0.01 to 100.00. The highest differences occurred in the abscissas of the centres of the vortices. The lowest percentage difference between the abscissas was 0.79% (Re = 25.00) and the highest was 13.70% (Re = 100.00). However, in relation to the ordinates of the centres of the vortices formed, the effect of the error factors was less visible: the percentage differences were lower, ranging from 0.01% (Re = 50.00) to 3.41%, for Re = 1.00 (Pinto, 2013).

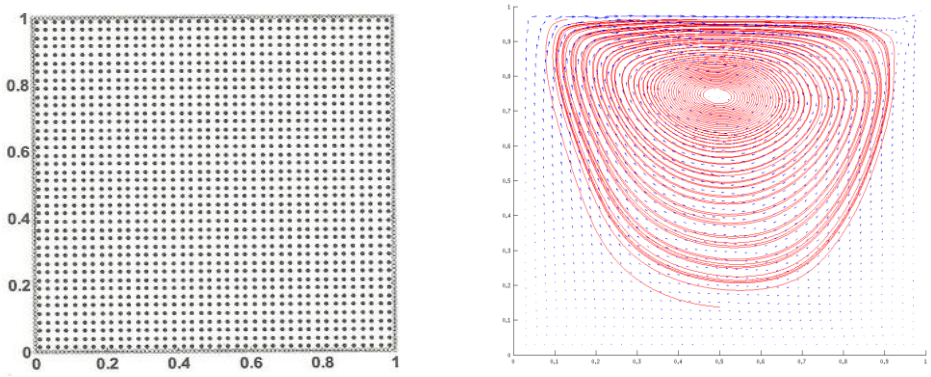

(a) (b)

Figure 9. (a) Initial particle distribution (40 × 40, inside the cavity) and virtual particles of type I (320, on the walls); (b) streamlines, velocity field, and primary vortex formed.

Figure 10 shows the comparison between the non-dimensional velocity profiles at the horizontal and vertical centrelines obtained by SPH and the velocity profiles from results reported in the literature (Marques and Doricio, 2006).

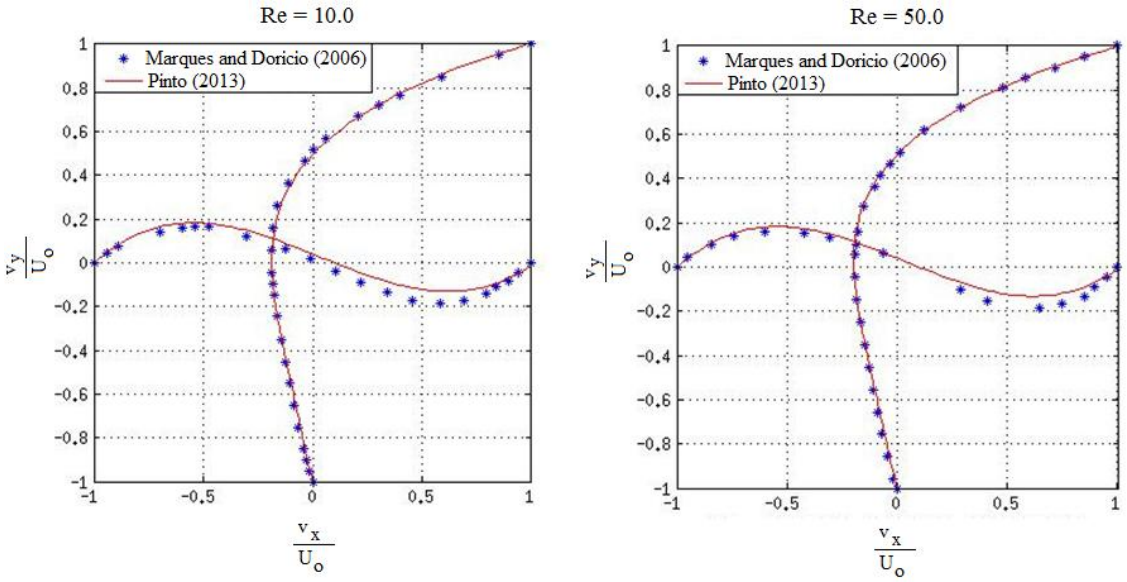

Figure 10. Differences between non-dimensional velocities at the horizontal and vertical centrelines (comparing SPH and results reported in the literature).

4.4. Propagation of a Water Wave over a Flat Beach

The problem of the propagation of a wave on a flat beach has been studied using two mathematical modellings: Lagrangian and Eulerian.

In the Lagrangian modelling, the SPH method has been used to solve the mass conservation and momentum balance equations. In the simulations, the open-source code SPHysics, developed as a collaboration between researchers from Johns Hopkins University (USA), the University of Vigo (Spain), and the University of Manchester (UK), has been employed. A detailed description of the code can be found in the SPHysics Manual (Gesteira et al., 2010).

The Eulerian modelling was based on Boussinesq-type equations for second-order dispersion, obtained after integration, in shallow waters, of the mass and momentum conservation equations in the vertical direction. To solve the partial differential equations that govern the movement of water, FUNWAVE 2D, a non-commercial software produced by the Centre for Applied Coastal Research (CACR, Delaware, USA), have been employed in the simulations. The numerical method implemented is the finite difference scheme, and an artificial eddy term is introduced into the equations to simulate the wave breaking (Fraga Filho et al., 2015).

A beach domain 2.75 m long in the inclined region, with an inclination angle of 4.2364°, amplitude and wave period of 0.01 and 1.4 s, respectively, and water level of 0.18 m, was simulated. For the generation of waves, a wave-maker was employed.

In the Eulerian simulation, a domain mesh with 156 nodes in the horizontal direction and 21 nodes in the vertical direction was used. The spacing between dots in the horizontal direction was 0.05 m. The origins of the frames of reference were coincident in Eulerian and Lagrangian simulations. In the Eulerian simulation, sponge layer boundary conditions has been used to damp the wave energy. The period was 30.00 s, with a time increment of 0.001 s during the simulations and the CFL number assumed a value of 0.20.

A cubic spline kernel was used in the Lagrangian simulation and 4221 fluid particles were employed to discretize the domain of interest from 0.00 to 3.75 m. The lateral distance between the centres of mass of two neighbouring particles was 0.01 m. The support radius (h) was defined as 0.013 m (approximately 1.30 times the initial spacing between the centres of mass of the particles). The virtual particle technique has been used to represent the fluid boundaries. To represent the fixed bottom of the channel, 387 particles of type I has been used, and to represent the motion of the flap-type wave-maker, 31 particles in a line were used. A time step of 4.5×10^{-5} s has been used in the simulation, carried out for a physical time of 30.00 s. Repulsion forces, analogous to the Lennard-Jones molecular forces, were exerted by the virtual particles on the fluid particles, keeping them inside the domain. A correction for the kernel truncation near the boundaries has not been made. The renormalization of the density of the fluid particles has been performed during the simulation. Large-eddy simulation (LES) has been employed to consider the turbulence effects in the SPH model. For the time integration, in both the Eulerian and the Lagrangian simulations, the predictor-corrector method has been used to generate a water wave of 0.02 m amplitude.

The free surface elevation has been obtained by the Lagrangian and Eulerian models (SPHysics and FUNWAVE 2D, respectively). In the Lagrangian model, the own fluid particles have defined the free surface at each simulated instant of time. Figure 11 shows the numerical results at 28.0 s.

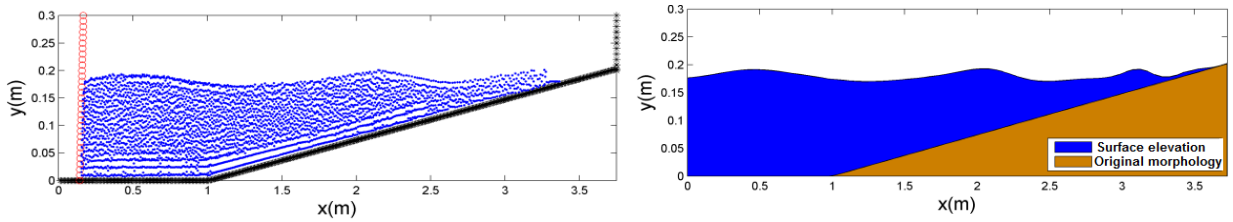

Figure 11. Simulation results. Left: the results of the SPHysics model; right: the results of the FUNWAVE 2D model.

Figure 12 shows the results for two models at 28.0 s in a single graphical representation. It can be observed that the results achieved by both methods presented a good concordance, mainly outside the surf zone, and some discrepancy on the slope near the shore.

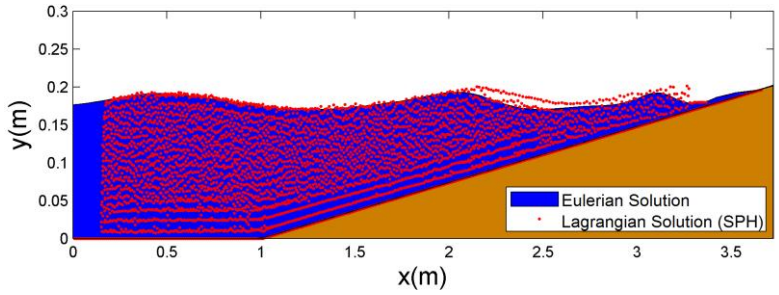

Figure 12. Graphical comparison of the results of the SPHysics and FUNWAVE 2D models at a simulation time of 28.0 s.

The Lagrange model has the advantage of showing the wave breaking in a very representative visual form, wherein the waveform may be visible through the movement of water particles. During the simulation, the waveform (defined by the water particles whose positions change over time) is visible and consistent with the physical phenomenon that is taking place.

The action of the breaking wave and run-up, rising wave on the beach, results in a highly complex movement (which is composed by medium and orbital motions, and also the turbulence), that have so far defied the precision of measurements and numerical modeling of coastal processes (Nwogu, 1996). From the analysis of Figs. 11 and 12, it can be concluded that the simulation results obtained from SPH, with the implementation of the repulsive boundary treatment, were consistent with the behaviour encountered by the finite difference scheme and sponge layer boundary conditions implemented in the Eulerian method.

4.5. Geometric Reflection and Dynamic Boundary Conditions

Virtual particles were employed and arranged in a staggered manner on the contours. The Dirichlet boundary condition was applied to the velocities of the virtual particles (zero). The computational domain consisted of a tank 4.00 m long and 4.00 m high, containing fluid that initially occupied a rectangular area with dimensions of 2.00 m × 1.00 m. Fluid particles were initially placed with a lateral separation between their centres of mass of 3.00 cm. A cubic kernel has been used. The time step was initialized equal to 1.0×10^{-4} s, which has varied throughout the simulation. The criteria presented by Gomez-Gesteira et al. (2010) has been employed in its calculating, in each numerical iteration. Figure 13 shows the geometry of the computational domain and the fluid discretization by particles.

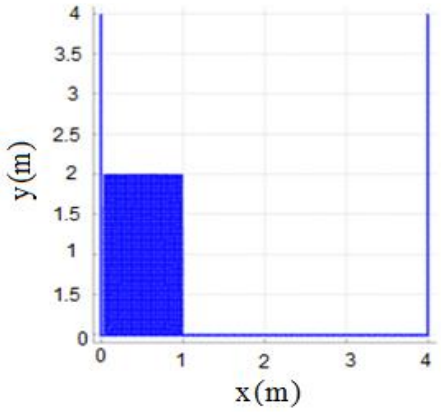

Figure 13. Geometry of the computational domain and fluid discretization by particles.

In the simulations of dynamic boundaries, the open-source code SPHysics was used. The validation of this code for use in dam breaking was carried out using laboratory experiments by Kleefsman et al. (2008), according to publications by Crespo et al. (2011) and Gomez-Gesteira et al. (2012).

In the simulations in which the geometric contours were employed, a numerical code developed and implemented by the authors of this work was used. The computational domain had the same geometry simulated with the use of dynamic boundaries. In the discretization of the fluid volume, 2556 particles were employed with an initial lateral separation between the centres of mass of 2.86 cm. The time step was 1.0×10^{-4} s (kept constant during the simulations). The fluid particles that formed the free surface were marked, and conditions of null pressure and constant pressure were applied to them. In the treatment of solid contours, planes (against which fluid particles collided and were reflected) were implemented. The coefficient of restitution of kinetic energy was equal to 1.00 (elastic collisions of particles against the planes). The kernel used was the cubic spline, presented by Liu and Liu (2010). The absolute pressure (P) on the particles presents terms related to the hydrostatic and dynamic pressures. The modified pressure concept, as presented by Batchelor (2000), has not been employed (it is not commonly employed in free surface flows). The estimation of the dynamic pressure field with the use of the Tait equation (term B had the value 0.85×10^5 Pa). The free surface particles have been marked and the constant pressure condition (zero) has been first applied and renewed in every numerical iteration. After the solution of Eq. (6), temporal integration for the position and velocity has been solved using the Euler method. The densities of the particles and the pressure gradients obtained by SPH interpolations were corrected by CSPM in each iteration. The experimental results presented by Cruchaga et al. (2007) were used to validate the numerical code implemented until the moment of the wave collision against the reservoir wall (Fraga Filho, 2014).

Figure 14 shows the wave front positions at time instants 0.40 and 0.80 s.

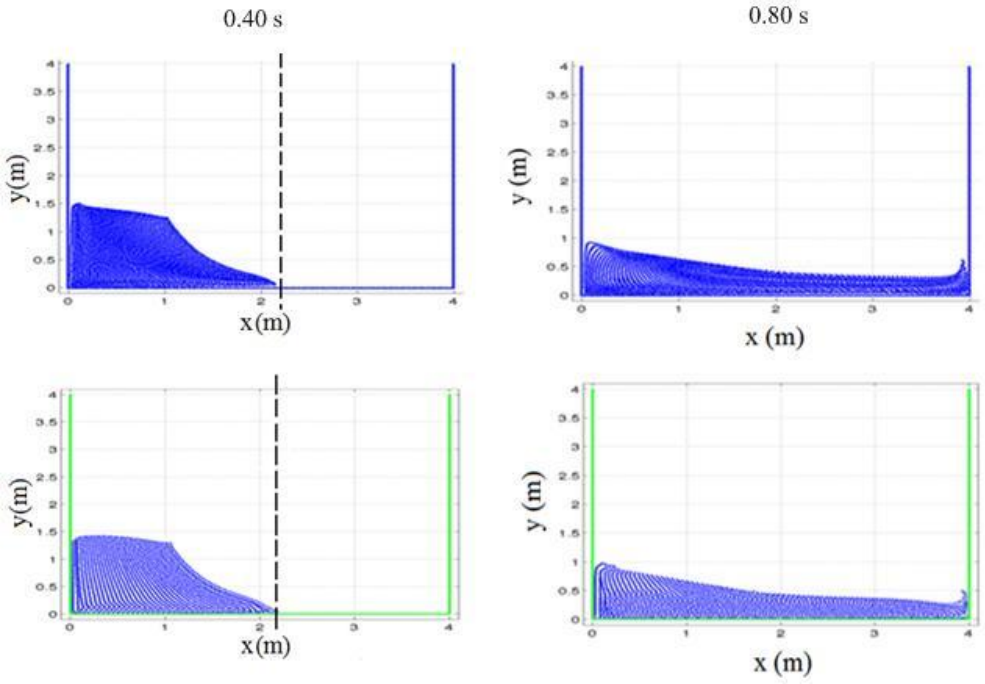

Figure 14. Wave front positions at time instants 0.40 and 0.80 s. (Top row: SPHysics simulations. Bottom row: simulations using the code implemented by the authors of this work).

The discrepancy between the wave fronts at the time instant 0.40 s was 2.86 cm, which is equivalent to a percentage difference of 2.5%. At the time instant 0.80 s, the height of the wave after the collision with the reservoir wall obtained with the code implemented in this work was 0.50 m, whereas that obtained with SPHysics was 0.60 m (the percentage difference was 16.66%). The results obtained with the use of both forms of boundary treatments showed good agreement.

5. CONCLUSIONS

In this paper, implementations of some boundary treatment methods in the Smoothed Particle Hydrodynamics (SPH) method were presented. In the case studies performed virtual particles, repulsive and dynamic conditions, and geometric contours were analysed.

In the study of heat diffusion in a flat plate, virtual particles were used in conjunction with Dirichlet boundary conditions. The numerical results were compared with the analytical solution. The results found by SPH show agreement with the analytical solution in remote regions of the lower boundaries of the plate. However, in regions close to the lower contours, kernel truncation and particle inconsistency were seen. One way to perform the correction of fluid properties in these areas is by using a correction factor (as shown in the CSPM).

In the hydrostatic problem presented (fluid at rest within an immobile reservoir), virtual particles in a region adjacent to the domain were used along with the modified pressure concept. The SPH results were excellent, being exactly equal to the analytical solution, and obeyed the continuum theory without the occurrence of undesirable oscillation of particles seen in other studies reported in the scientific literature.

In the shear-driven cavity, the repulsive boundary conditions were tested. Virtual particles were fixed on the contours and the repulsive force exerted by the virtual particles on the fluid particles, calculated by analogy with the Lennard-Jones molecular force, has been implemented. The numerical results obtained by SPH were concordant with the results provided by the literature.

In the study of the generation and propagation of a wave, Eulerian and Lagrangian mathematical modellings were employed. In the Lagrangian referential, repulsive boundary conditions have been used, as in the previous case. Sponge layer conditions has been employed in the Eulerian modelling. The numerical results obtained by both models showed agreement with regard to the behaviour of the elevation of the free surface throughout the beach area. The SPH method, with employment of repulsive boundary conditions, led to a good solution to the problem studied.

Finally, dynamic and geometric boundary conditions were employed in the dam breaking simulations. The results showed good agreement before the shock wave against the reservoir wall, which led to the conclusion that both the boundary conditions can be applied in simulations of dam breaking using the SPH method.

In summary, different boundary conditions were implemented and tested to verify their applicability to the case studies. Through comparisons of the numerical results with analytical, experimental, and literature results (despite the good results achieved using different boundary treatment techniques), it was found that there was no unique or general SPH boundary treatment for those problems. In each problem studied there was a need to perform numerical tests or to study computational implementations previously performed in order to define which boundary conditions could be applied.

REFERENCES

Batchelor, G.K., 2000. *An Introduction to Fluid Dynamics*. Cambridge University Press, 3rd edition, Cambridge, UK.

Chen, J.K., Beraun, J. E., & Carney, T.C., 1999. A Corrective Smoothed Patricle Method for Boundary Value Problems in Heat Conduction. *International Journal for Numerical Methods in Engineering*, 46: 231-252.

Courant R., Friedrichs K., & Lewy H., 1967. On the partial difference equations of mathematical physics. *IBM Journal*, 11:215-234.

Crespo A.J.C., Dominguez J.M., Barreiro A., Gomez-Gesteira M., & Rogers B.D., 2011. GPUs, a new tool of acceleration in CFD: efficiency and reliability on Smoothed Particle Hydrodynamics methods. *PLoS ONE* 6 (6). Available at: http://journals.plos.org/plosone/article?id=10.1371/journal.pone.0020685 [Acessed: 25 June 2016].

Cruchaga M.A., Celentano D.J., & Tezduyar T.E., 2007. Collapse of a liquid column: numerical simulation and experimental validation. *Comput. Mech.*, 39: 453-476.

Ferrand M., Laurence D. R., Rogers B. D., Violeau D., & Kassiotis C., 2013. Unified semi-analytical wall boundary conditions for inviscid, laminar or turbulent flows in the meshless SPH method. *International Journal for Numerical Methods in Fluids*, 71(4): 446-472.

Fourtakas, G., Vacondio, R., & Rogers, B.D., 2015. On the approximate zeroth and first-order consistency in the presence of 2-D irregular boundaries in SPH obtained by the virtual boundary particle methods. *International Journal Numerical Methods in Fluids, published online in Wiley Online Library (wileyonlinelibrary.com)*.

Fraga Filho, C.A.D., & Chacaltana, J.T.A., 2014. Numerical Study of Heat Diffusion Employing the Lagrangian Smoothed Particle Hydrodynamics Method: an Analysis of the Applicability of the Laplacian Operator and the Influence of the Boundaries on the Solution. *International Review on Modelling and Simulations (I.RE.MO.S.)*, 2014, vol. 7, N. 6, pp. 994-1002.

Fraga Filho, C.A.D., 2014. Estudo da Fase Gravitacional-inercial do Espalhamento de Óleo em Mar Calmo empregando o Método Lagrangiano de Partículas Smoothed Particle Hydrodynamics. PhD Thesis, Federal University of Espírito Santo, Brazil. Available at: http://cfd.mace.manchester.ac.uk/sph/SPH_PhDs/2014/Carlos_Alberto_DUTRA_FRAGA_FILHO_PhD_Thesis_2014.pdf [Accessed: 20 March 2016].

Fraga Filho, C.A.D, Piccoli, F. P., Barbosa, D.A. & Chacaltana, J.T.A., 2015. Estudo numérico da propagação de ondas em praias planas utilizando os modelos *Lagrangiano* sem malhas e Euleriano. *Revista Brasileira de Recursos Hídricos*, vol. 20, nº 1, pp. 91-105.

Gingold, R. A., & Monaghan, J. J., 1977. Smoothed Particle Hydrodynamics: Theory and Application to Non-spherical stars. *Monthly Notices of the Royal Astronomical Society*, vol. 181, pp. 375-338.

Gomez-Gesteira, M., Rogers, B.D., Crespo, A.J.C., Dalrymple, R.A., & Narayanaswamy, M., 2010. *User Guide for SPHysics Code*. Available at: https://wiki.manchester.ac.uk/sphysics/images/SPHysics v2.2.000 GUIDE.pdf [Acessed: 25 June 2016]

Gomez-Gesteira M., Crespo A.J.C., Rogers B.D., Dalrymple R.A., Dominguez J.M., & Barreiro A., 2012. SPHysics development of a free-surface fluid solver Part 2: Efficiency and test cases. *Computers & Geosciences*, 48:300-307.

Kleefsman K.M.T., Fekken G., Veldman A.E.P., Iwanowski B. & Buchner B.A., 2008. Volume-of-Fluid based simulation method for wave impact problems. J. Comput. Phys. 206: 363-393.

Kulasegaram S., Bonet J., Lewis R., & Profit M., 2006. A variational formulation based contact algorithm for rigid boundaries in two-dimensional SPH applications. *Computational Mechanics*, 33(4): 316-325.

Leroy, A., Violeau D., Ferrand M., & Kassiotis C., 2014. Unified semi-analytical wall boundary conditions applied to 2-D incompressible SPH. *Journal of Computational Physics*, 261:106-129.

Liu G.R., & Liu M.B., 2003. *Smoothed particle hydrodynamics: a meshfree particle method*. World Scientific, Singapore.

Liu, M.B., & Liu, G.R, 2010. Smoothed Particle Hydrodynamics (SPH): an Overview and Recent Developments. *Archives of Computational Methods in Engineering*, 17: 25-76.

Lucy, L.B., 1977. Numerical approach to testing the fission hypothesis. *Astronomical Journal*, 82: 1013-1024.

Marques, A.C.H., & Doricio, J. L., 2006. Numerical investigation of the flow in a two-dimensional cavity: Meshless, Finite Volumes and Finite Difference Methods. *Latin American Journal of Solids and Structures*, vol.3, pp. 301-324.

Monaghan, J.J., 1992. Smoothed Particle Hydrodynamics. *Annual Review of Astronomy and Astrophysics*, vol. 30, pp. 543-574.

Nwogu, O. G., 1996. Numerical Prediction of Breaking Waves and Currents with a Boussinesq Model. *Proceedings of the 25th International Conference on Coastal Engineering*, ICCE '96, Orlando, Vol. 4, 4807-4820.

Pinto, W.J.N., Fraga Filho, C.A.D., & Chacaltana, J.T.A., 2011. Aplicação do Método Lagrangiano SPH (Smoothed Particle Hydrodynamics) para a Solução do Problema das Cavidades. *Anais do XIV Encontro de Modelagem Computacional (XIV EMC) e do II Encontro de Ciência e Tecnologia de Materiais (II ECTM).* Nova Friburgo: Editora: Rede SIRIUS, Universidade do Estado do Rio de Janeiro, vol. 01, pp. 500-508.

Pinto, W.J.N. *Aplicação do Método Lagrangiano SPH (Smoothed Particle Hydrodynamics) para a Solução do Problema das Cavidades*, 2013. Masters Dissertation, Federal University of Espírito Santo (UFES), Brazil.

Pletcher, R.H., Tanehill, J.C., & Anderson D.A. 1997. *Computational Fluid Mechanics and Heat Transfer*, Taylor and Francis, 2nd edition, London, UK.

Rapaport D.C., 2004. *The art of molecular dynamics simulation*. Cambridge University Press, 2nd edition, Cambridge, UK.

Vaughan G.L., Healy, T.R., Bryan, K.R., Sneyd A.D., & Gorman, R. M., 2008. Completeness, conservation and error in SPH for fluids. *International Journal for Numerical Methods in Fluids*, vol. 56, pp. 37–62.